Optically pumped wavelength-tunable lasing from a GaN beam cavity with an integrated Joule heater pivoted on Si

Feifei Qin(秦飞飞)[1], Yang Sun(孙阳)[1], Ying Yang(杨颖)[1], Xin Li(李欣)[1,2], Xu Wang(王旭)[3], Junfeng Lu(卢俊峰)[4], Yongjin Wang(王永进)[1], and Gangyi Zhu(朱刚毅)[1,†]

[1] *GaN Optoelectronic Integration International Cooperation Joint Laboratory of Jiangsu Province, College of Telecommunications and Information Engineering, Nanjing University of Posts and Telecommunications, Nanjing* 210003, *China*

[2] *Key Laboratory of Broadband Wireless Communication and Sensor Network Technology (Nanjing University of Posts and Telecommunications, Ministry of Education), Nanjing* 210003, *China*

[3] *Department of Microelectronic Science and Engineering, School of Physical Science and Technology, Ningbo University, Ningbo* 315211, *China*

[4] *College of Physics, Nanjing University of Aeronautics and Astronautics, Nanjing* 211106, *China*

(Received 13 December 2022; revised manuscript received 11 February 2023; accepted manuscript online 2 March 2023)

Dynamically tunable laser sources are highly promising for realizing visionary concepts of integrated photonic circuits and other applications. In this paper, a GaN-based laser with an integrated PN junction heater on Si is fabricated. The photoluminescence properties of the GaN beam cavity are controlled by temperature, and the Joule heater provides electrically driven regulation of temperature. These two features of the cavity make it possible to realize convenient tuning of the lasing properties. The multi-functional GaN beam cavity achieves optically pumped lasing with a single mode near 362.4 nm with a high Q-factor of 1394. The temperature of this device increases by 0–5 °C under the Joule heating effect. Then, electrical control of the lasing mode is demonstrated. The lasing resonant peak shows a continuous redshift of about 0.5 nm and the device also exhibits dynamic switching of its lasing mode. The lasing modulation can be ascribed to temperature-induced reduction of the bandgap. Our work may be of benefit for external optical modulation in future chip-based optoelectronic devices.

Keywords: GaN beam cavity, optically pumped lasing, dynamically tunable laser source, Joule heater

PACS: 42.25.Bs, 28.52.Fa, 42.55.–f **DOI:** 10.1088/1674-1056/acc05e

1. Introduction

GaN microcavity lasers integrated monolithically on silicon platforms have attracted considerable interest in many research areas. The performance of GaN microdisk lasers has been greatly limited by material qualities, processing techniques and significant optical loss caused by optical coupling to the sapphire substrate or through rough sidewalls.[1,2] High-quality GaN materials are usually grown on a sapphire substrate. With a focus on material growth, the quality of Si-based GaN epitaxial wafers has been considerably improved. Although still not good enough, Si-based GaN materials can now also fit the requirement for lasing.[3,4] With the development of standard micro/nanofabrication technologies, including lithography and dry etching, high-quality GaN microcavity lasers on Si substrates have been designed and fabricated.[5–8] Suspension of the device can reduce the optical loss. For example, Zhang *et al.*[9] have reported optically pumped lasing from 2 μm GaN microdisks pivoted on Si. To *et al.*[10] obtained a GaN microdisk with a direct coupled waveguide. Accompanied by the intensive development of Si-based GaN microcavity lasers, several types of cavity lasing modulation have also been demonstrated, such as single-mode lasing,[11] emission direction control[12,13] and on-chip integration.[14,15] More importantly, the capability for wide-range tuning of the stimulated emission of these devices is still a key issue for the high performance of future on-chip applications. Much effort needs to be made to develop convenient mode manipulation strategies.

In the past years, tremendous progress has been made in the realization of wavelength-tunable lasers. For example, static wavelength tailoring has been realized in specially designed cavities such as compound cavities,[16,17] cavities with a distributed Bragg reflector[18] and coupled[19–21] or asymmetric cavities.[12,22] Apart from static wavelength tuning, GaN cavity lasers also exhibit the potential for excellent dynamic wavelength operation due to their optical–electrical characteristics, such as a high piezoelectric coefficient,[23] high electro-optical coefficient[24] or high thermo-optical coefficient.[25] Piezoelectric-induced lasing modulation has been reported in GaN microwires[26] and continuous electro-optic guided mode adjustability has been obtained in Si/GaN microring resonators.[14,27] Compared with others methods, thermal modulation is a more convenient way to realize mode control. However, most reported works, including our previous work,[28] are based on an external heating stage. An integrated internal heat source is more attractive, since it can make the system much simpler and more efficient.

Here, an optically pumped Fabry–Pérot (F-P) mode laser with a floating GaN beam structure is fabricated via a stan-

†Corresponding author. E-mail: zhugangyi@njupt.edu.cn

© 2023 Chinese Physical Society and IOP Publishing Ltd

dard micro/nanofabrication process. Spontaneous and stimulated radiation under optical pumping of the GaN beam cavity is studied. A Joule heater is introduced to the device as an internal heat source by designing an InGaN PN junction structure. The GaN beam cavity is multifunctional, with both a PN junction heater and a lasing cavity. Joule heating under electrical control can effectively tailor the optical properties of the cavity. In this case, photoluminescence (PL) of the GaN beam cavity proved to have a relationship with Joule heating of the cavity. The optically pumped lasing properties, resonant mode simulation and Joule heat-induced lasing mode evolution of the device will be studied later. Our results indicate that single-mode lasing tuning and mode switching for these cavities can be realized in a simple experimental environment (voltage below 5 V, current < 30 mA).

2. Experimental details

2.1. Fabrication of GaN microcavity

With a process similar to one used previously,[29,30] a beam structured GaN cavity is fabricated on a Si substrate (Fig. 1(g)). To simplify the introduction of the PN junction to the resonant cavity, a light-emitting diode (LED) epitaxial wafer is used as the basic material. The wafer consists of an AlN layer (2.1 μm), an undoped GaN layer, an n-GaN layer (1.5 μm), an AlGaN layer (1.3 μm with 3%–10% Al), a GaN/InGaN quantum well (QW) multi-layer (50 nm with 10% In) and a p-GaN layer (550 nm). This design makes it possible to realize the combination of a PN junction heater and lasing resonant cavity in a single device. The fabrication process of the GaN lasing structure is illustrated in Figs. 1(a)–1(f).

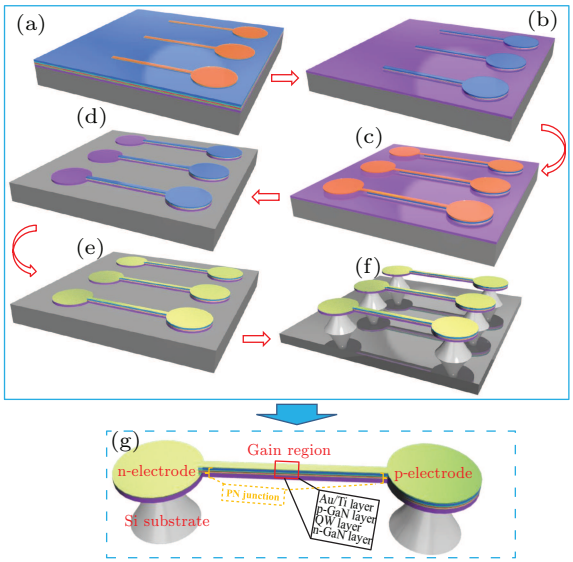


Fig. 1. Fabrication process for the GaN beam structure on a Si substrate: (a) patterning the photoresist for the p-GaN layer, (b) etching the n-GaN layer, (c) patterning the photoresist layer for the n-GaN layer, (d) etching the Si substrate, (e) patterning the photoresist layer and preparing the electrode, (f) wet isotropic etching of the silicon. (g) Final structures of the GaN beam cavity. The PN junction heater region and gain region on the GaN beam are marked.

The device is patterned with residual photoresist (step (a)) then etched on the n-GaN layer by inductively coupled plasma (ICP) etching (step (b)). The GaN beam and two electrode holders are patterned (step (c)), then etched to the Si layer (step (d)). Subsequently, the p- and n-electrodes (20 nm Ti and 100 nm gold) are prepared on the n-GaN and p-GaN layers by patterning and electron beam evaporation (step (e)). Finally, the entire structure is wet etched by a solution of HF and HNO_3 (HNF) until the silicon substrate is shaped into columns to support the GaN beam devices (step (f)). With these methods, a GaN beam cavity array pivoted on Si is obtained. As demonstrated in Fig. 1(g), the PN junction remained in our final device. Joule heating is easy to generate in a PN junction[31,32] and this can improve the electrical tuning abilities of the laser.

2.2. Sample characterization

The morphological properties of the samples are characterized by field emission scanning electron microscopy (Carl Zeiss Ultra-Plus) and confocal microscopy (Zeiss, Observer.DIM). Optical properties, including the temperature-dependent PL spectra, lasing spectra and threshold values for our GaN cavity, are measured by a confocal micro-PL setup (Olympus BX35) excited by a 355 nm femtosecond pulsed laser or a 405 nm picosecond laser. The pumping light covers as much of the GaN beam cavity as possible. The excitation laser is focused onto the top surface of the GaN beam through a 40× objective lens to the central position. The spot diameter of the pumping light is about 30 μm in this case. The PL spectra are resolved by a spectrometer (Princeton Instruments Acton SP2500i). Since the device is bonded to the printed circuit board (PCB) substrate, current injection in this case is easy. The GaN beam is driven by a commercial source meter (Agilent B2901) to produce Joule thermal heating. Temperature distribution of the chip is simultaneously recorded by a thermal imager (VC320).

3. Results and discussion

3.1. Structural and optical properties of GaN beam cavity

Through a special design, a beam-like GaN cavity can be realized. The top SEM image of an individual GaN beam in Fig. 2(a) indicates that the GaN beam has a width of approximately 24.7 μm, a thickness of about 5.5 μm and is supported by two circular GaN disks with diameters of about 150 μm. The entire structure is floated on a Si substrate to reduce optical loss. The side view of an individual GaN cavity in Fig. 2(c) shows that the GaN beam cavity is suspended. From top to bottom, the entire device comprises a metal electrode (Ti and Au), p-GaN layer, QW layer, n-GaN layer and silicon substrate. All these layers mean that the PN junction remains in the final structures. Since the GaN layer is thick enough, the

whole cavity can serve as both a lasing cavity (under optical pumping) and a Joule heater (electrically driven). As shown in Fig. 2(b), the top diameter of the Si pedestal is about 90 μm. Since the diameter of the GaN microdisk is about 150 μm, the etching radii should be greater than 30 μm.[33] Optical loss in this case will be reduced. This benefits the realization of optically pumped lasing. The details of the cavity are shown at greater magnification. A step gap of approximately 500 nm is left between the p and n areas to prevent any short-circuiting [Fig. 2(d)]. The separated layers of the p and n areas and the electrode area are shown at greater magnification in Fig. 2(e). The GaN beam cavity array can be made by standard processing technology and these devices are bound to the PCB substrate [inset in Fig. 2(f)] for further measurements.

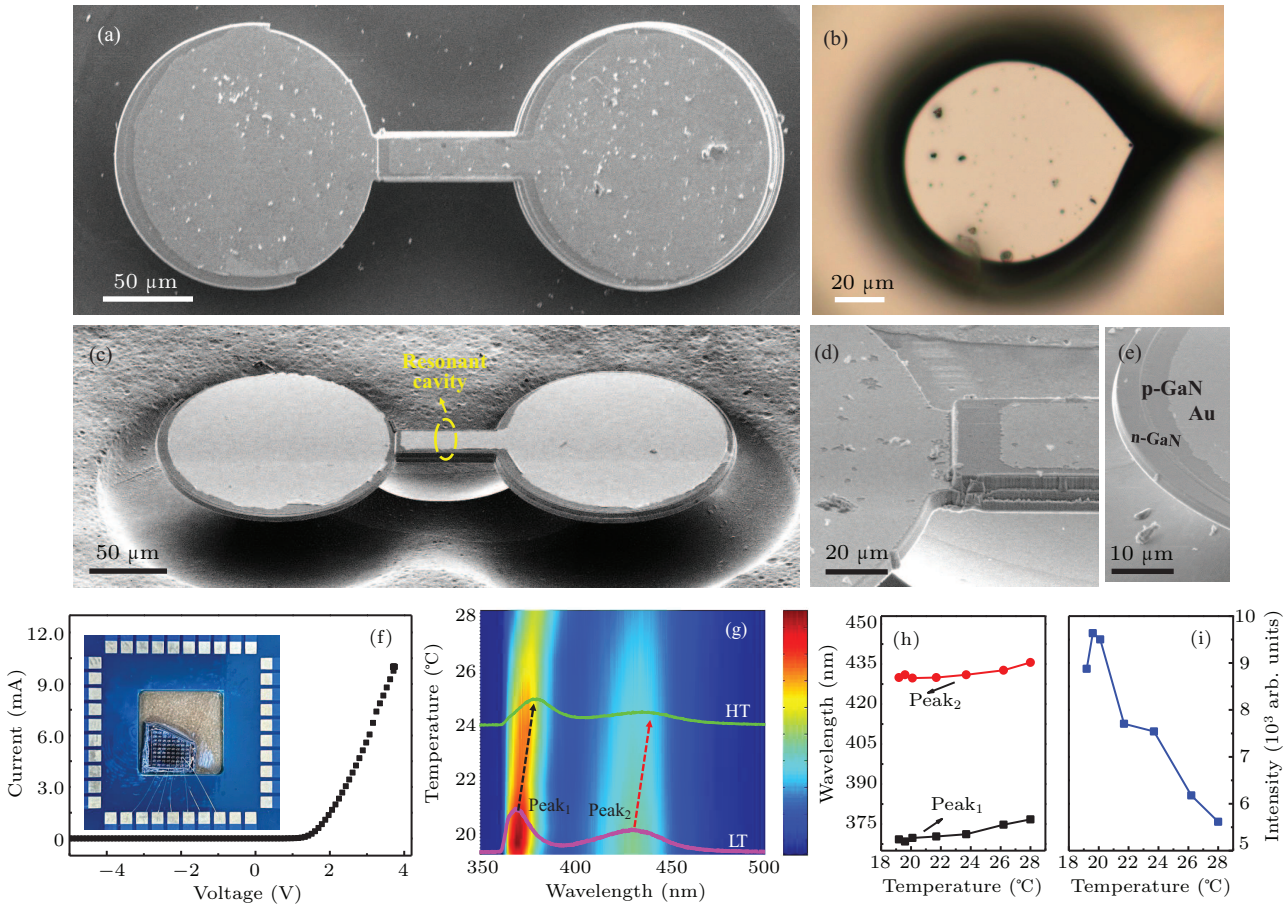


Fig. 2. (a) Top view of an individual GaN beam structure. (b) Charge-coupled device image of the Si pedestal after removing the GaN layer. (c) Side view of an individual GaN beam structure. (d), (e) Enlarged images of the side region and gap region. (f) Current–voltage (I–V) curves of the GaN beam structure; the inset shows GaN beam arrays bonded to the PCB substrate. (g) Temperature-dependent PL spectra of the GaN beam cavity (fixed pumping power of 96 μW) under Joule heating (HT, high temperature; LT, low temperature). (h) Peak wavelength and (i) PL intensity from PL spectra of GaN beam cavity at different temperatures.

The current–voltage (I–V) characteristic curves of the individual structures are plotted in Fig. 2(f). The device exhibits obvious rectification characteristics with a turn-on voltage of approximately 2 V. This I–V curve confirms that the PN junction exists in the GaN cavity and is smaller than that of a normal GaN LED.[34,35] Besides, electroluminescence (EL) spectra of part of the GaN beam cavities can also be observed. The corresponding EL spectra results are shown in Fig. S1. With an increase in the injection current from 0 mA to 22 mA, the main emission of the device peaks at 451 nm. In addition, as shown in Fig. S1(b), the EL intensity increases with the addition of a drive current.

Coincidentally, by changing the fabrication process, devices with controllable EL properties can be obtained. The injected electrical power converts into heat in two major ways: nonradiative recombination from the active region and the Joule heat from the p-type layers.[36] If the device is not an emitter, most carriers will transform to nonradiative recombination. Thus, the trick is that the Joule heat-induced temperature increase is more obvious for the device without EL and only these devices are suitable for conducting the optical pumping lasing experiment.

With the increase in drive current, the Joule effect will increase the temperature of the GaN cavity. A GaN beam cavity with spontaneous emission is chosen to study Joule heat-induced PL modulation. Under 355 nm laser pumping (at a fixed pumping power of 96 μW) the device shows two main peaks at low temperature, as seen in Fig. 2(g). One is in the ultraviolet region, with a peak near 370 nm, belonging to near-band-edge emission of GaN.[37] The other is in the blue region

with a peak near 430 nm, belonging to the emission of the QW layers. A clear PL shift is observed at high temperature. As shown in Fig. 2(h), the electrically driven Joule heat-induced improvement in temperature is about 10 °C. In this case the main peaks are gradually redshifted to 376 nm and 435 nm, respectively. The PL intensity decreases significantly with increasing temperature in Fig. 2(i). This entire phenomenon fits the features of thermal reduction of the bandgap and PL quenching of the GaN cavity.

3.2. Lasing properties of an individual GaN beam cavity

A GaN device with stimulated radiation is chosen to demonstrate optically pumped lasing and lasing mode-tuning experiments. The optically pumped lasing properties of an individual GaN beam are investigated under 355 nm laser pumping. Figure 3(a) shows the high-resolution spectra collected at different pumping powers of the individual GaN beam cavity. At 1.77 μW, weak spontaneous radiation is observed. When the pumping power increases to 3 μW, single-mode lasing appeared, with a peak wavelength near 362.4 nm and full width at half maximum (FWHM) of 0.26 nm. Using

$$Q = \lambda/\Delta\lambda, \tag{1}$$

the Q-factor is 1394. Further increase in the excitation power increases the lasing intensity, but no clear mode evolution appears.

The threshold curve in Fig. 3(b) indicates that the threshold value of this cavity is about 3 μW. As shown in Fig. 3(c), the FWHM of PL decreases with the addition of pumping power for spontaneous radiation below the threshold, and it changes sharply to about 0.26 nm for pumping powers above the threshold. Further increase in the pumping power will slightly increase the FWHM. Considering the cavity structures in Fig. 2(a) the spectral properties in Fig. 3(a) and the dark emission image inserted in Fig. 3(a), the most possible mechanism for lasing here is the F-P resonance mode in the wide direction of the GaN beam. The wavelength of the resonant mode in this type of resonator is expressed as

$$\lambda = 2nL/m, \tag{2}$$

where n is the refractive index, L the cavity length and m the resonant mode. The free spectral range (FSR) is given by

$$\mathrm{FSR} = \lambda^2/2L(n - \lambda\,\mathrm{d}n/\mathrm{d}\lambda), \tag{3}$$

where $\mathrm{d}n/\mathrm{d}\lambda$ is the dispersion of the refractive index.

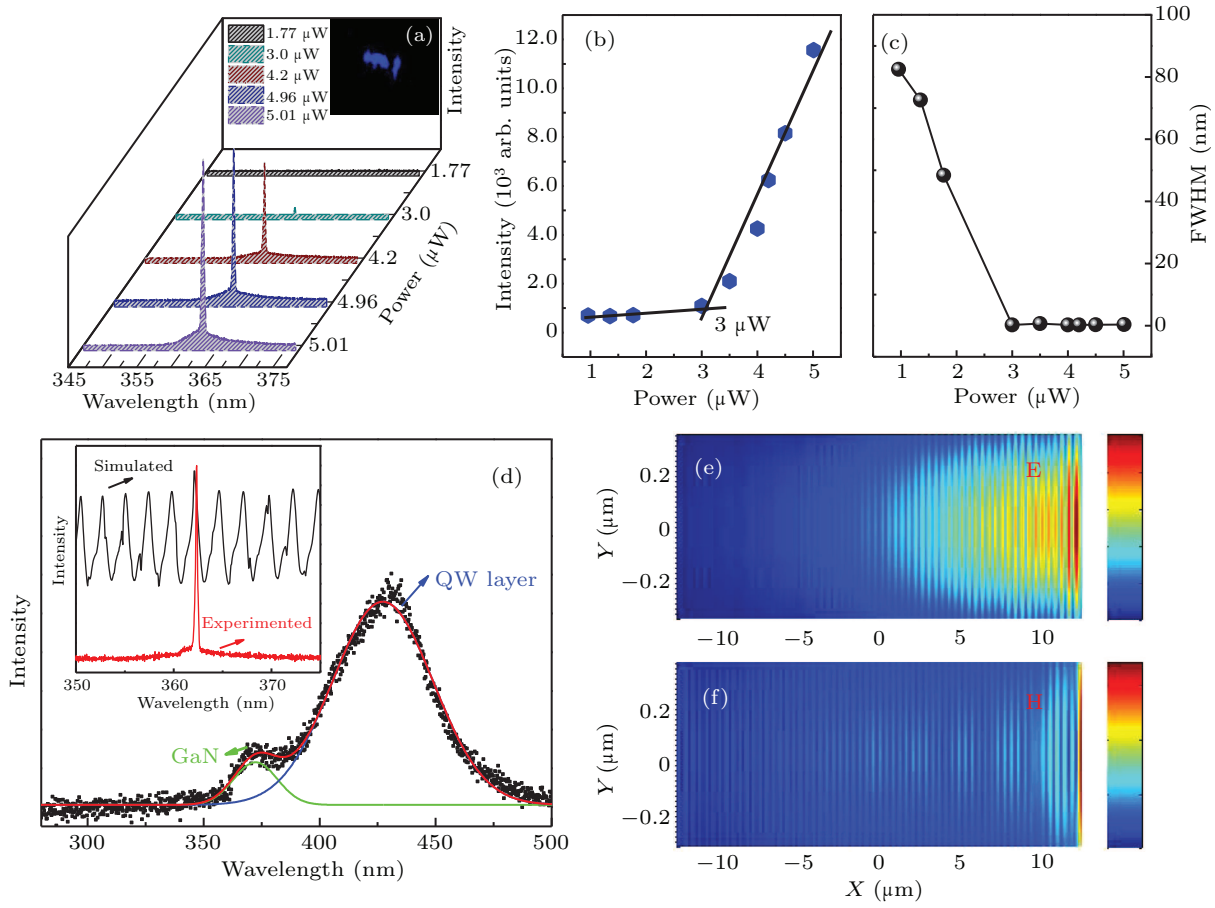


Fig. 3. (a) Lasing properties of the optically pumped laser. The inset shows the dark charge-coupled device image. (b) Threshold curves and (c) FWHM summary of an individual GaN beam cavity. (d) PL spectra of a GaN epitaxial wafer on Si. The inset shows the simulated resonant mode of a GaN F-P cavity with a width of 24.7 μm and normalized lasing spectra. (e), (f) Simulated electromagnetic field distribution for a GaN F-P cavity with resonant mode near 362.4 nm.

As shown in the inserted charge-coupled device image in Fig. 3(a), the F-P mode optical field distribution with a strip of light path is obtained. The single-mode lasing is due to the loss of metal. Due to breaks in the surface of the Au layer, light can also escape through the top surface of the cavity. The lasing oscillation and F-P mode optical field distribution are more obvious when the surface metal layer is removed (shown in Fig. S2). This shows images of a clear strip of light path and resonant modes near 364.1 nm, 365.3 nm, 366.3 nm and 363.8 nm.

To clarify the origin of the lasing mode, PL from the same sample is measured and plotted in Fig. 3(d). Gaussian fitting of the PL peaks confirms the similar peaks shown in Fig. 2(g). Moreover, our samples show a dependence on excitation wavelength. As shown in Fig. S3, PL under 355 nm laser pumping shows a PL peak near 370 nm that belongs to emission from n-GaN, and PL under 405 nm laser pumping implies a PL peak near 450 nm. This should be due to emission from p-GaN.

Comparing the data in Figs. 3(a), 3(d), and S3, we can see that the gain region of lasing resonance is in the ultraviolet, and it belongs to n-GaN. To further confirm the resonant mechanism, finite-difference time-domain simulation of F-P lasing based on the gain region in Fig. 3(d) and cavity size in Fig. 2(a) are carried out (see the supplementary materials for details of the simulation methods). A clear resonant mode appears for the F-P resonant cavity, as shown in Figs. 3(e) and 3(f). Comparison of the experimental lasing spectra in Fig. 3(a) and the simulated lasing oscillation inserted in Fig. 3(c) implies that they should originate from the same resonant series. An interesting phenomenon is that, as the simulation results imply, for a F-P cavity with a length of 24.7 μm, many resonant modes should appear. However, during the experiment, only a single mode or a few modes of lasing appear in the GaN beam cavity. This can be attributed to the optical loss induced by the surface metal and self-absorption causing mode suppression.

3.3. Joule heat-induced lasing mode modulation

Joule heat from a PN junction usually has a negative influence on the emission of InGaN LEDs[38,39] and it can be used as a thermal source to modulate the optically pumped lasing of the GaN beam cavity. The experimental setup shown in the inset to Fig. 4(c) is used to study the optically pumped lasing performance of the GaN structure shown in the insert to Fig. 4(b) as Joule heat varied. Lasing with a resonant mode near 362.35 nm and FWHM of 0.27 nm is observed in Fig. 4(a). With the pumping power fixed, applying a current to the GaN cavity resulted in the lasing mode being highly redshifted. If the drive current is above 10 mA, the resonant mode will be changed to another resonant mode series and then it will be redshifted again. At a drive current of 20 mA, a mode near 364.6 nm appears, and it becomes the main peak at 25 mA. The details can be seen in the summary of the peak wavelength and FWHM of the resonant modes in Fig. 4(b). The FWHM increases with addition of the drive current, with the resonant peak redshifted from 362.35 nm to 362.73 nm (drive current below 10 mA), then blueshifted to 362.47 nm (drive current at 15 mA).

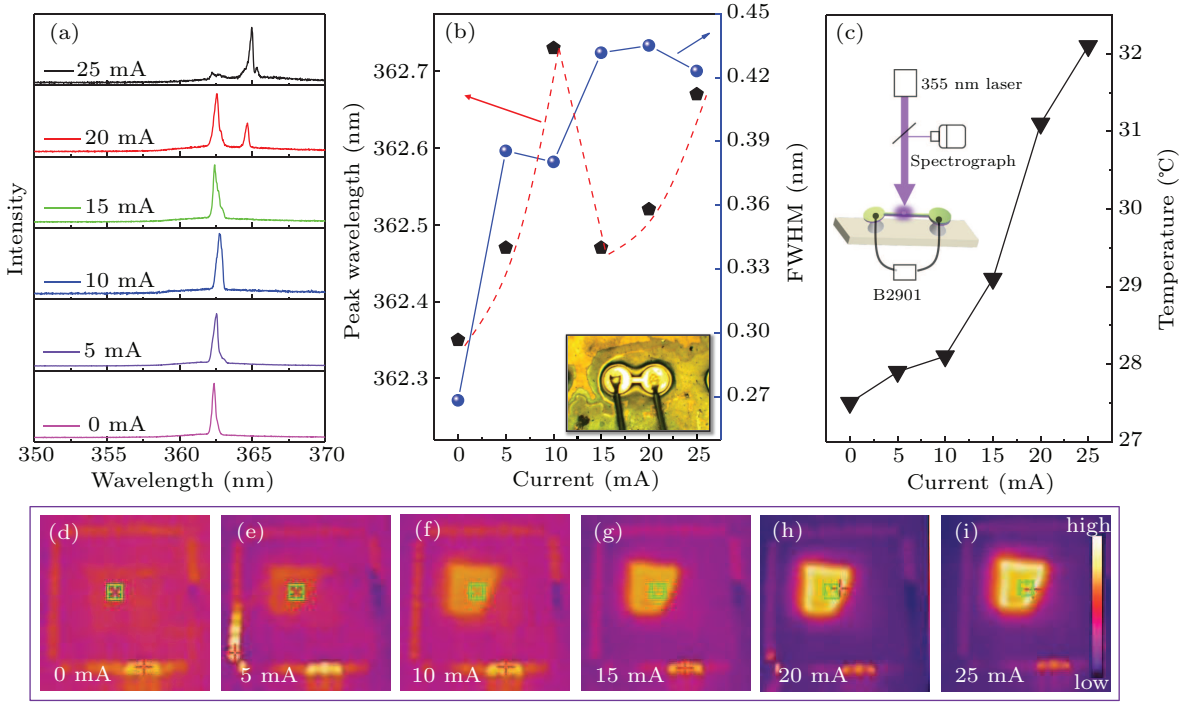


Fig. 4. (a) Drive-current-dependent lasing properties of the GaN cavity while the pumping power is fixed. (b) Peak wavelength and FWHM summary of (a): the inset shows a charge-coupled device image of an individual GaN beam cavity with its bound line. (c) Peak temperature of the device under different drive currents: the inset shows the experimental setup of wavelength tunable lasing. (d)–(i) Current-dependent temperature field distribution.

It also seems that the peak wavelength of the lasing mode is not monotonously changing with the injected current in Fig. 4(b). The abnormal blueshift of the resonant mode at 15 mA can be explained by the well-known mode-hopping behavior. In this case, the increase in temperature influences mode competition and make the detected light move to another mode. The redshift of the resonant mode can be attributed to the temperature-induced gain shift of the cavity.[40–42] The increased temperatures shown in Figs. 4(d)–4(i) support this assumption. Temperature changes in this case are about 0–5 °C [Fig. 4(c)].

More interestingly, in addition to the static mode modulation in Fig. 4(a), the mode-switching phenomenon can also be realized for a sample with high temperature tunability. As shown in Fig. 5, optically pumped lasing with a peak wavelength of 363.6 nm is obtained. The lasing modes can be divided into three different regions. While applying Joule heat to the device, the single-mode lasing peak is tuned in the region of 363.6 nm to 370.3 nm for a drive current below 25 mA. For a drive current of approximately 30 mA, the main mode changes to 373.8 nm, and multi-mode lasing appears. In this situation, clear mode switching is realized by applying a suitable drive current, as presented in Fig. S4.

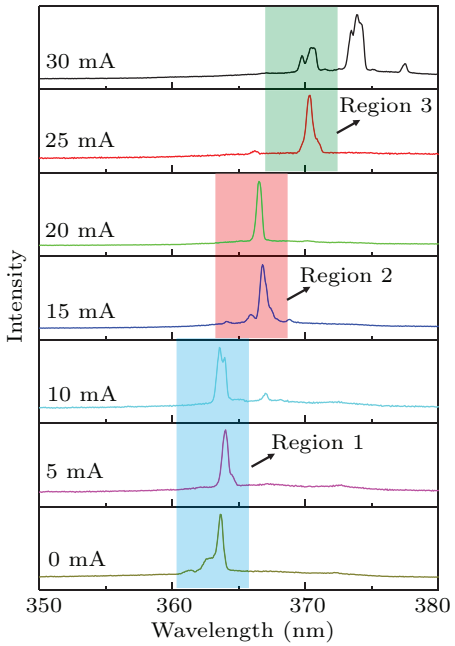


Fig. 5. Demonstration of the lasing mode switch in the optimized structure.

4. Conclusion

In summary, a Si-based GaN beam cavity is designed and fabricated using standard semiconductor technology. F-P type single-mode lasing peaked near 362.4 nm and a *Q*-value of 1394 under 355 nm laser pumping is realized. More importantly, by using a Si-based InGaN LED epitaxial wafer as the gain material and designing a special PN junction structure, the GaN beam cavity served as both a lasing cavity and an internal Joule heating source. A controllable temperature change is realized for the GaN device as the drive current increases, thus controlling the PL properties of the multi-functional cavity. We demonstrate a wavelength-tunable laser via an electric tuning scheme. Joule heating is the main contributor to the spectral engineering. In this case, the lasing of the GaN cavity is tuned with a redshift at the nanometer scale and mode switching at several nanoscales. Overall, the proposed GaN beam laser provides a method for future chip-based optoelectronic applications to tune the performance of GaN microdisk lasers.

Acknowledgements

Project supported by the Natural Science Foundation of Jiangsu Province, China (Grant No. BK20210593), the Foundation of Jiangsu Provincial Double Innovation Doctor Program (Grant No. 30644), the National Natural Science Foundation of China (Grant No. 62204127), State Key Laboratory of Luminescence and Applications (Grant No. SKLA 202104), open research fund of Key Lab of Broadband Wireless Communication and Sensor Network Technology (Nanjing University of Posts and Telecommunications, Ministry of Education).

References

[1] Zhang Y, Zhang X, Li K H, Cheung Y F, Feng C and Choi H W 2015 *Phys. Status. Solodi A* **212** 960
[2] Chang S, Rex N B, Chang R K, Chong G and Guido L J 1999 *Appl. Phys. Lett.* **75** 3719
[3] Feng M, Liu J, Sun Q and Yang H 2021 *Prog. Quant. Electron.* **77** 100323
[4] Liu J, Wang J, Sun X, Sun Q, Feng M, Zhou R, Zhou Y, Gao H, Liu T, Huang Z and Yang H 2019 *ACS Photonics* **6** 2104
[5] Zhang X, Cheung Y F, Zhang Y and Choi H W 2014 *Opt. Lett.* **39** 5614
[6] Ghosh P, Yu D, Hu T, Liang J, Chen Z, Yingkai L and Huang M 2019 *J. Mater. Sci.* **54** 8472
[7] Feng M, Wang J, Zhou R, Sun Q, Gao H, Zhou Y, Liu J, Huang Y, Zhang S, Ikeda M, Wang H, Zhang Y, Wang Y and Yang H 2018 *IEEE J. Sel. Top. Quant.* **24** 1
[8] Xing Z Q, Zhou Y J, Liu Y H and Wang F 2020 *Chin. Phys. Lett.* **37** 027302
[9] Zhang Y, Ma Z, Zhang X, Wang T and Choi H 2014 *Appl. Phys. Lett.* **104** 221106
[10] To C H, Fu W Y, Li K H, Cheung Y F and Choi H W 2020 *Opt. Lett.* **45** 791
[11] Yang Y, Wei T, Zhu R, Zong H, Lu J, Li J, Liao H, Yu G, Pan C and Hu X 2018 *Opt. Express* **26** 30021
[12] Zhang S, Li Y, Hu P, Tian Z, Li Q, Li A, Zhang Y and Yun F 2021 *Photonics Res.* **9** 432
[13] Zhang S, Li Y, Hu P, Li A, Zhang Y, Du W, Du M, Li Q and Yun F 2020 *Opt. Express* **28** 6443
[14] Zhang Y G, Tian Z B, Zhang X Y, Zhang X J, Gu Y, Li A Z, Zhu X R, Zheng Y L and Liui S 2007 *Chin. Phys. Lett.* **24** 2839
[15] Tabataba-Vakili F, Alloing B, Damilano B, Souissi H, Brimont C, Doyennette L, Guillet T, Checoury X, El Kurdi M, Chenot S, Frayssinet E, Duboz J Y, Semond F, Gayral B and Boucaud P 2020 *Opt. Lett.* **45** 4276
[16] Xu Z, Tong J, Shi X, Deng J and Zhai T 2020 *Polymers* **12** 656

[17] Li M, Gan J, Zhang Z, Lin W, Zhao Q, Xu S and Yang Z 2018 *Opt. Commun.* **420** 1

[18] Zhou D B, Liang S, Han L S, Zhao L J and Wang W 2017 *Chin. Phys. Lett.* **34** 034204

[19] Xu H, Wright J B, Luk T S, Figiel J J, Cross K, Lester L F, Balakrishnan G, Wang G T, Brener I and Li Q 2012 *Appl. Phys. Lett.* **101** 113106

[20] Liu C W, Zhang J C, Yan F L, Jia Z W, Zhao Z B, Zhuo N and Wang Z G 2017 *Chin. Phys. Lett.* **34** 034209

[21] Yang K, Yang Y D, Xiao J L and Huang Y Z 2022 *Chin. Phys. B* **31** 094205

[22] Li Y, Feng L, Li F, Hu P, Du M, Su X, Sun D, Tang H, Li Q and Yun F 2018 *ACS Photonics* **5** 4259

[23] Lueng C M, Chan H L W, Surya C, Fong W K, Choy C L, Chow P and Rosamond M 1999 *J. Non-Cryst. Solids* **254** 123

[24] Long X C, Myers R, Brueck S, Ramer R, Zheng K and Hersee S 1995 *Appl. Phys. Lett.* **67** 1349

[25] Watanabe N, Kimoto T and Suda J 2012 *Jpn. J. Appl. Phys.* **51** 112101

[26] Peng Y, Lu J, Peng D, Ma W, Li F, Chen Q and Pan C 2019 *Adv. Funct. Mater.* **29** 1905051

[27] Thubthimthong B, Sasaki T and Hane K 2018 *Appl. Phys. Lett.* **112** 071102

[28] Qin F, Zhu G, Wang R, Wang X, Lu J, Yang Y and Qiu G 2021 *J. Phys. D Appl. Phys.* **54** 255103

[29] Zhu G, Tian M, Almokhtar M, Qin F, Li B, Zhou M and Wang Y 2022 *Chin. Phys. Lett.* **39** 123401

[30] Wang J, Feng M, Zhou R, Sun Q, Liu J, Sun X, Zheng X, Sheng X and Yang H 2020 *Appl. Phys. Express* **13** 074002

[31] Yang X, Shan Z, Luo Z, Hu X, Liu H, Liu Q, Zhang Y, Zhang X, Shoaib M, Qu J, Yi X, Wang X, Zhu X, Liu Y, Liao L, Wang X, Chen S and Pan A 2020 *ACS Nano* **14** 3397

[32] Wang J, Feng M, Zhou R, Sun Q, Liu J, Sun X, Zheng X, Sheng X and Yang H 2020 *Appl. Phys. Express* **13** 074002

[33] Zhang Y, Huang J A, Li K H, Bai D, Wang Y, Wang T and Choi H 2016 *J. Phys. D Appl. Phys.* **49** 375103

[34] Ra Y H and Lee C R 2020 *Nano Lett.* **20** 4162

[35] Yan F, Jiang Y, Sun X, Wei J, Chen L and Zhang Y 2019 *Nano Res.* **13** 52

[36] Mei Y, Xu R B, Xu H, Ying L Y, Zheng Z W, Zhang B P, Li M and Zhang J 2017 *Semicond. Sci. Tech.* **33** 015016

[37] Qin F, Zhu Q, Zhang Y, Wang R, Wang X, Zhou M and Yang Y 2021 *Opt. Mater.* **122** 111663

[38] Efremov A, Bochkareva N, Gorbunov R, Lavrinovich D, Rebane Y T, Tarkhin D and Shreter Y G 2006 *Semiconductors* **40** 605

[39] Choi I, Lee K, Lee C R, Lee J S, Kim S M, Jeong K U and Kim J S 2019 *Acs Appl. Mater. Interf.* **11** 18876

[40] Leroux M, Grandjean N, Beaumont B, Nataf G, Semond F, Massies J and Gibart P 1999 *J. Appl. Phys.* **86** 3721

[41] Fujiwara H, Niyuki R and Sasaki K 2018 *J. Phy. Commun.* **2** 035022

[42] Wang Q, Yan Y, Qin F, Xu C, Liu X, Tan P, Shi N, Hu S, Li L, Zeng Y, Zhao Y and Jiang Y 2017 *NPG Asia Mater.* **9** e442